Mathematical Monographs
vol. 9 (2016), pp. 75-88

# Behavior analysis of coating layer particles in cosmetic materials during drying by observation and computational simulation

Katsuyuki HASEGAWA, Akio NASU, Masahiro FUJITA

**Abstract.** The most of liquid foundations contain volatile solvents. So the particles states in foundations can also change in drying process after application. On the other hand, the macroscopic appearance of foundation applied skin depends on the microscopic particles states on skin surface. To understand how the particles behave in coating layers during drying, observations of slurries and computational simulation of particles behavior was performed. As a result, it is confirmed that a weak van der Waals force and slow drying speed have advantage to particles spread on substrate.

## 1. Introduction

The most important function of makeup products is to make the face look beautiful and, of all of the makeup components, this function is primarily owing to powder. Many kinds of powder have been developed for this purpose [1–13], and recent studies have also examined the influence that the microscopic distribution of powder on the surface of the skin has upon the macroscopic appearance of the skin [14‑15]. Tsugita reported that the reflectivity of the make-up skin increases with the thickness of the foundation coating and follows the diffuse reflectance of the foundation by the analysis of make-up skin using visible RGB-LED optical coherence tomography [14]. Katsuyama showed that the attachment of powder foundation to peripheral portion of the pore is effective to make the pore inconspicuous by the experiment using skin model composed of polyurethane and the computational simulation based on geometrical optics [15]. It was evident that different types of dispersion of the powder particles on skin produced different appearances, even when the same powder composition was applied to the same skin. However, the relationship between each component and the particle arrangement on the skin surface has not been thoroughly investigated until now. This unpredictable appearance of the skin is especially true for products such as liquid foundation containing volatile ingredients that create a composition change during the drying process post-application and, as a result, the initial dispersed condition of the particles in the bulk slurry is not necessarily maintained on the skin after drying. Therefore, it has been difficult to predict the final particle distribution on the skin from the bulk formulation. By gaining a deeper understanding of the structure formation mechanism during drying, however, it should be possible to determine the properties needed for each ingredient to obtain the desired final arrangement of the particles. That is, the formula of liquid foundation can be designed corresponding to

the appearance of make-up skin demanded.

It is assumed that the process of using a liquid foundation is one wherein a film is formed by the deposition and drying of a colloidal dispersion in a volatile solvent on a substrate. The wet process for film formation is a basic industrial technology used in various fields such as printing [16–17], electronics [18–19] and foods [20]. Particularly in printable electronics, the complicated patterning and fine structure of nanoparticles by means of a wet process have been recently investigated [21–23]. It is difficult to determine the dynamics of the structure formation only by experimental methods, however, which makes it challenging to clarify the mechanism of the film formation and drying. Fujita et al. have developed a three-dimensional structure formation simulator for colloidal nanoparticles during drying in which the motion of nanoparticles are visualized with time and the structure can be evaluated [24–25].

In this study, to clarify how particle structure formed during drying, each particle behavior in a coating layer was observed experimentally and simulated by computer.

## 2. Experiments

### 2.1. Materials

A mixture of one powder and one volatile oil was used for the observation sample. Two powders were selected, comprising spherical particles with a mean diameter of approximately 5 μm and a narrow particle size distribution, wherein one was composed of polydimethylsiloxane (PDMS; MOMENTIVE PERFORMANCE MATERIALS INC. JAPAN, Tokyo, Japan) and the other of polymethyl-methacrylate (PMMA; TOYOBO CO., LTD., Osaka, Japan). For the volatile oils, four oils with different drying speeds and surface tensions were selected. Low molecular weight dimethylsilicone (WACKER ASAHIKASEI SILICONE CO., LTD., Tokyo, Japan) and isododecane (MARUZEN PETROCHEMICAL CO. LTD., Tokyo, Japan) were used as high drying speed oils, while cyclopentasiloxane (MOMENTIVE) and isohexadecane (PRESPERSE INC., NJ, USA) were used as low drying speed oils. The powders and oils were mixed into a slurry in a homogenizer (PT-MR 2000, KINEMATICA, Luzern, Switzerland) at a 1 to 4 ratio.

### 2.2. Observation

All observations were performed using a transmitted light microscope (BX-60, Olympus, Tokyo, Japan) equipped with a fully focusing image pickup device (Focuscope FV-100C, PHOTRON, Tokyo, Japan). To obtain focused object images that are focused for every pixel, a plurality of object images were photographed at different focus positions and the focused pixels were stitched together into one image, which accurately generated all-in-focus images. Each slurry was applied to a glass slide with a 20 μm thickness using a bar coater, and the drying process of each coating layer was observed at room temperature. The objective lens was made to vibrate vertically by width of 40 μm by a piezoelectric actuator to obtain all-in-focus images from the bottom to the surface of the coating.

## 3. Computational simulation

For the computational simulation of particles in a slurry, we used a simulation program (SANP-L) based on the Brownian dynamics model developed by Fujita et al. [24–25], with the SNAP-L model given below. Particles, assumed as rigid spheres, moving in a slurry receive various forces from other particles, the substrate and the solvent. The translational motion of the *i*th particle is expressed by

$$m_i \frac{\partial v_i}{\partial t} = F_i^{\mathrm{co}} + F_i^{\mathrm{ca}} + F_i^{\mathrm{e}} + F_i^{\mathrm{vdw}} - \xi v_i + R_i, \tag{1}$$

where $m$ is the mass of the particle, $t$ is time, $v$ is the translational velocity vector, $R$ is the Brownian random force vector, $\xi$ is the coefficient of Stokes drag for a particle, $F^{\mathrm{co}}$ is the contact force vector, $F^{\mathrm{ca}}$ is the capillary force, $F^{\mathrm{e}}$ is the electrostatic force vector, and $F^{\mathrm{vdw}}$ is the van der Waals force vector. The rotational motion of the *i*th particle obeys the angular momentum conservation law

$$I_i \frac{\partial \omega_i}{\partial t} = T_i^{\mathrm{co}}, \tag{2}$$

where $I$ is the inertial moment of the particle, $\omega$ is the angular velocity vector and $T^{\mathrm{co}}$ is the contact torque vector. The contact force and torque between two particles are modeled according to the discrete element method (DEM), which is the method typically used in the field of particulate media mechanics. The electrostatic and van der Waals forces obey the DLVO (Derjaguin-Landau-Verwey-Overbeek) theory [26], and the capillary force is given as a combination of the lateral capillary immersion force and the vertical capillary force, such that

$$F_i^{\mathrm{ca}} = \sum_j f_{ij}^{\mathrm{l}} n_{ij} + f_i^{\mathrm{v}} s_i \tag{3}$$

where $f^{\mathrm{v}}$ is the vertical force, $f^{\mathrm{l}}$ is the lateral force, $\boldsymbol{n}$ is the unit vector connecting centers of spheres and $\boldsymbol{s}$ is the unit vector normal to the interface. The lateral capillary force is generated by deformation of the meniscus when another particle protruding from the interface is nearby. The magnitude of the lateral capillary force is approximately given by Kralchevsky and Nagayama [27].

$$f_{ij}^{\mathrm{l}} = {2\pi\gamma Q^2}\Big/{L_{ij}} \tag{4}$$

where

$$\mathrm{Q} = r_c \sin\psi \tag{5}$$

where $L_{ij}$ is distance between centers of two spheres, $\gamma$ is surface tension, $r_c$ is radius of an interface circle on a sphere $\Psi$ is slope angle of an interface on a sphere. the slope angle depends on the contact angle and the height of the interface. On the other hand, vertical capillary force is exerted on all spheres that protrude the interface, and is given by

$$f_i^{\mathrm{v}} = 2\pi\gamma Q \tag{6}$$

The basic parameters used for the numerical calculation are shown in Table 1, wherein the solvent in this study is the oil used. All calculations were performed

with the condition that the ζ-potential was 0 mV because the electrostatic force should be negligible. To reduce the calculation load, the scale of the entire system was reduced and the particle size was set as 0.1 μm, which is smaller than that of the particles in the actual samples. Two drying speeds of $5.0\times10^{-2}$ and $5.0\times10^{-3}$ m/s were used, and two Hamaker constants of $5.0\times10^{-19}$ and $5.0\times10^{-20}$ J were examined in these simulations.

Table 1. Parameters used for the SNAP-L simulations

| | | |
|---|---|---|
| particle | ζ potential | 0 mV |
| | Friction coeffient | 0.01 |
| | Contact angle | 60 ° |
| | Hamaker constant | $5x10^{-20}$ or $1x10^{-20}$ J |
| | Number of particles | 139 particles<br>(1.0 as coverage on substrate) |
| | Diameter of particle | 0.1 μm |
| solvent | Coefficient of viscosity | 1 mPa・s |
| | Surface tension | 30 mN/m |
| | Drying speed | $5x10^{-2}$ or $5x10^{-3}$ m/s |
| | Initial height | 0.4 μm |

The value of the non-dimensional boundary area (NBA), which is a ratio for the exposure of a particle surface, was evaluated as the degree of dispersion and is expressed by [28]

$$\mathrm{NBA} = \frac{1}{cN}\sum_{k=0}^{c}(c-k)n(k), \tag{7}$$

where $c$ is the maximum coordination number, $N$ is the total number of particles and $n(k)$ is the number of particles whose coordination number is $k$. Note that $c$=12 for three dimensions. The NBA becomes 1 when all particles are completely dispersed, and it becomes 0 when all particles are in a hexagonal close packed arrangement.

## 4. Results

### 4.1. Observation of slurry drying process

Figure 1 shows the change during drying undergone by each slurry containing PDMS particles, wherein similar particle behaviors are confirmed regardless of the

solvent species. Initially, the agglomerations grow as the condensation of the slurry is followed by solvent evaporation. At the final stage of the drying process, the aggregates collapse and become extremely spread out on the substrates. After the particles temporarily organize into their closest packing on the plane, a portion of the voids in the packing structure expand slightly in the final drying state.

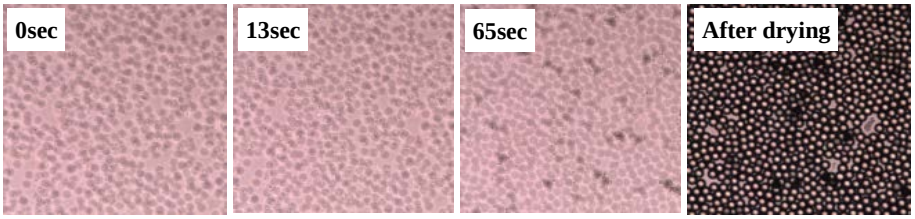


(a) Low molecular dimethylsulicone

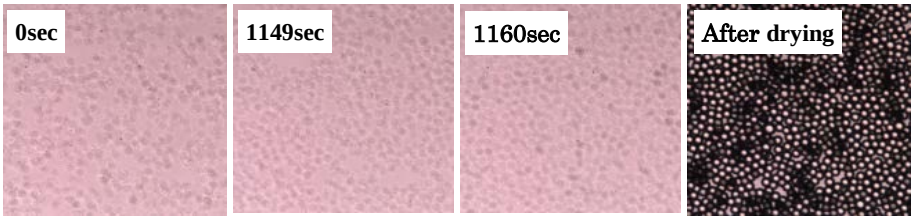


(b) Cyclopentasiloxane

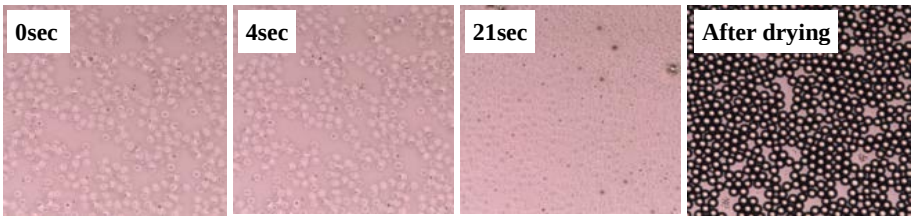


(c) Iso dodecane

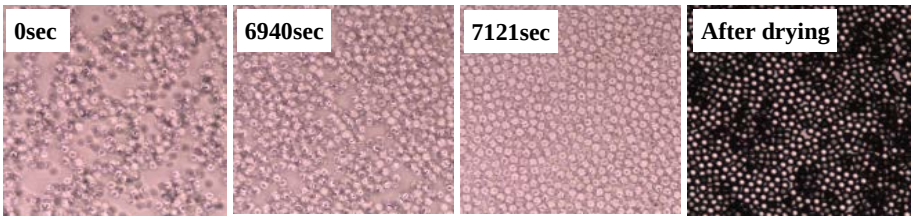


(d) Isohexadecane

Figure1. Microscope images showing the arrangement of polydimethylsiloxane (PDMA) particles during the drying process of slurries using a solvent of (a) low molecular weight dimethylsilicone, (b) isododecane, (c) cyclopentasiloxane and (d) isohexadecane.

The results of slurries containing PMMA are shown in Fig. 2 where, initially in

the drying process, there are no distinct differences between the different slurries, and the movements of the PMMA aggregates are slow and do not shift significantly from their initial positions. However, at the final drying stages, the slurries exhibit different behaviors depending upon the drying speeds of the solvents. In the cases of the less volatile solvents of cyclopentasiloxane and isohexadecane, the PMMA aggregates collapse and the particles spread more extensively than is true for the more volatile solvents. After the drying of the low volatile slurries, the particle coverage on the substrate surfaces is greater than that of the high volatile slurries.

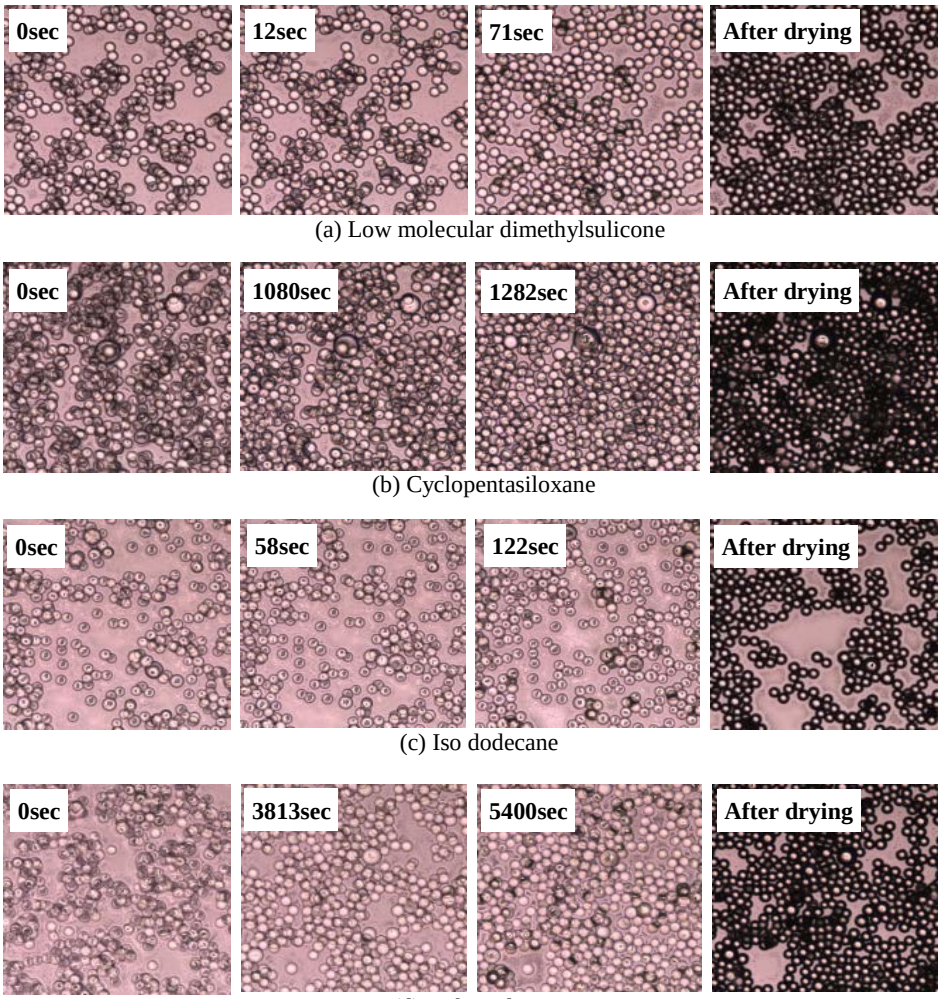


Figure 2. Microscope images showing the arrangement of polymethylmethacrylte (PMMA) particles during the drying process of slurries using a solvent of (a) low molecular weight dimethylsilicone, (b) isododecane, (c) cyclopentasiloxane and (d) isohexadecane.

### 4.2. Computational simulation of particle behavior in slurry

For computational simulation of the drying process, two initial particle conditions were arranged, where the first is a fully dispersed condition (Fig. 3(a)) in which all particles were placed with no interparticle contact, and the other is an aggregated state (Fig. 4(a)). To form the particle aggregates for the initial states, the calculation was performed under a drying speed condition of 0 m/s until the NBA value became constant.

For the fully dispersed condition, the simulation results with a high Hamaker constant ($5\times10^{-20}$ J) are shown in Figs. 3(b)–3(e), where there is no distinct difference between the aggregations after drying in a high volatile condition ($5\times10^{-2}$ m/s, Fig. 3(c)) and a low volatile condition ($5\times10^{-3}$ m/s, Fig. 3(e)), though the area of the cavities on the substrate are slightly smaller in the high volatile condition than in the low volatile condition. This result is opposite that observed in the PMMA slurries.

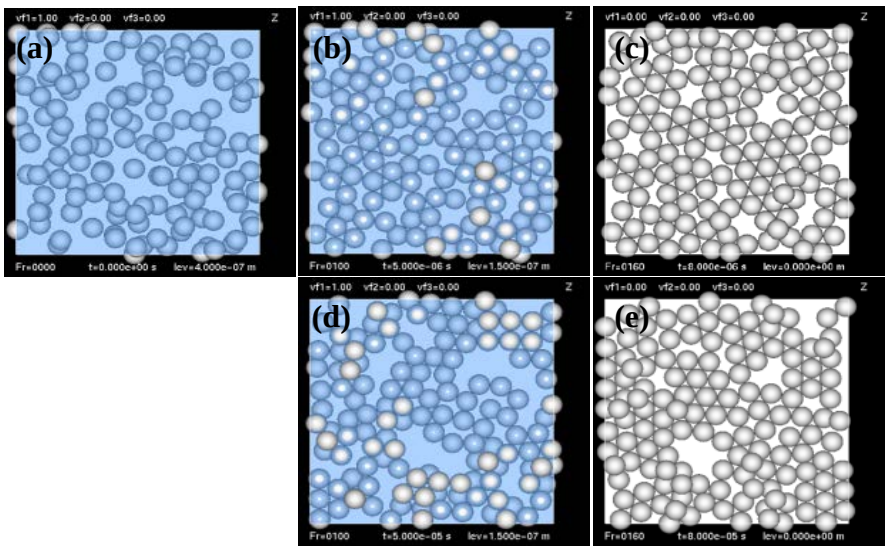


Figure 3. Computational simulation images of the drying process created using the fully dispersed state initial condition at (a) the initial state; (b) at a solvent height of 1.5 ×*d* and (c) after fully drying using the solvent drying speed of $5\times10^{-2}$ m/s; and (d) at a solvent height of 1.5 ×*d* and (e) after fully drying using the solvent drying speed of $5\times10^{-3}$ m/s. The parameter *d* is the particle diameter.

For the aggregated state initial condition, the simulation results with a high Hamaker constant ($5\times10^{-20}$ J) are shown in Figs. 4(b)–4(e). The particle coverage on

the substrate after drying under a high volatile condition ($5\times10^{-2}$ m/s, Fig. 4(c)) is seen to be less than that under a low volatile condition ($5\times10^{-3}$ m/s, Fig. 3(e)).

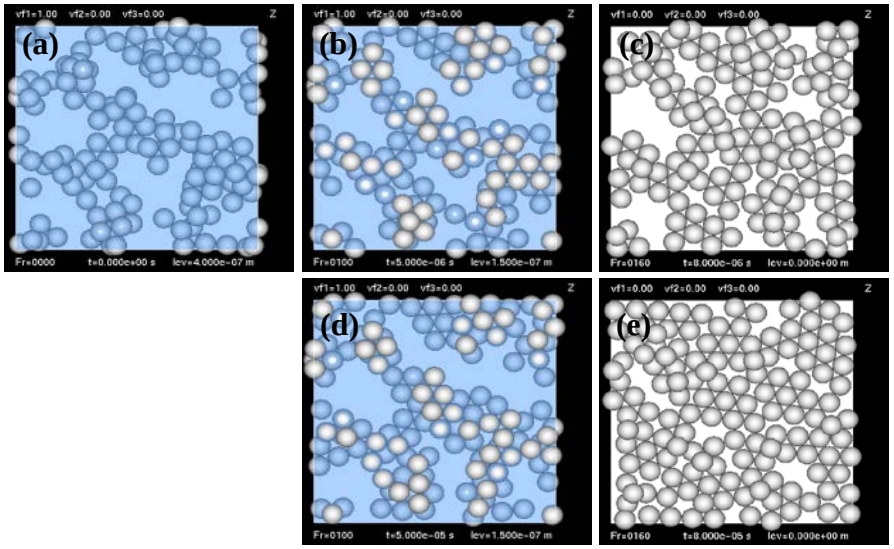


Figure 4. Computational simulation images of the drying process created using the aggregated state initial condition at (a) the initial state; (b) at a solvent height of 1.5 $\times d$ and (c) after fully drying using the solvent drying speed of $5\times10^{-2}$ m/s; and (d) at a solvent height of 1.5 $\times d$ and (e) after fully drying using the solvent drying speed of $5\times10^{-3}$ m/s. The parameter $d$ is the particle diameter.

These simulations are performed again using a low Hamaker constant ($1\times10^{-20}$ J), and images of the particle arrangements after drying are shown in Fig. 5. The degree of particle dispersion on the substrates after drying are seen to be similar and highly ordered whether the drying speed is derived from a high volatile condition (Fig. 5(a)) or a low volatile condition (Fig. 5(b)).

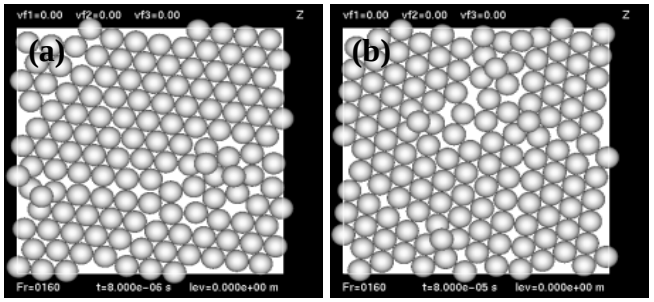


Figure 5. Computational simulation images after fully drying using a low Hamaker constant and a solvent drying speed of (a) $5\times10^{-2}$ and (b) $5\times10^{-3}$ m/s.

## 5. Discussion

### 5.1. Observation of slurry drying process

Using the observation results, in the drying process of the PDMS particle slurries, the magnitude of the van der Waals force between two silicone particles is dominant in the particle arrangement after drying. The cohesive force is very weak, however, because of the weak van der Waals force that exists between silicone surfaces, so aggregates composed of silicone PDMS particles can easily break with the addition of small external forces. This explains the insignificant differences in the drying of PDMS samples with various solvent volatilities and surface tensions. On the other hand, in the drying process of the PMMA particle slurries, the volatility of the solvent is seen to significantly change the aggregation structure during the drying process. The cohesive force between PMMA particles is stronger than between silicone particles and, to collapse the aggregates, a sufficient external force is required to deform the aggregates beyond the limit of elasticity. A slow drying speed means that any external forces are applied to the aggregates for a long time, and it is believed that this is the reason PMMA particles become well spread out in the slurry containing the low volatility solvent.

In all of the experiments, the organization of the particle structures are seen to change drastically in the last stages of drying. It is presumed that these changes do not occur in the inner parts of the coating layers, but on the surface where the particles protrude. That is to say, the vertical component of the capillary force generated by the capillary phenomena at the interface between the particles and the solvent is the force that presses the aggregates to the substrate. In actuality, the capillary force is the only external force that can break the aggregate structure in this simple system. Hydrocarbon solvents have a higher surface tension than silicone solvents, so it is expected that hydrocarbon solvents generate a larger capillary force to push the aggregates to the substrate. However, we observed no distinct change as a function of the solvent surface tension. It is supposed that an extremely large capillary force caused by a high surface tension will be able to break the aggregates, even though the drying speed is fast, but there is no oil possessing a higher volatility that is available for cosmetic products, so it is difficult to verify this hypothesis experimentally. For this case, therefore, the analysis of particle behaviors in the drying process was attempted using computational simulation.

### 5.2. Computational simulation of particle behavior in slurry

As the index of the degree of dispersion, the change of the NBA values over the drying process using the dispersed state as the initial condition is evaluated in Fig. 6. To compare the aggregations in the slurries containing different volatile solvents, the NBA value of the slurry is plotted as a function of the ratio ($H/d$) of the solvent height ($H$) to the particle diameter ($d$). At the initial drying stage, each particle does not touch any other particle, so the NBA value is 1. Subsequently, particles form aggregates and the NBA values therefore decrease until the solvent height reaches 1.2–1.3 $\times d$, regardless of the solvent volatility. Comparing the curves at identical solvents heights, the NBA values in the slow drying condition are seen to be lower

and the aggregates larger. The potential curve between the particle surfaces based upon the DLVO theory as a function of the inter-surface distance is illustrated in Fig. 7. In this study, the electrostatic force is assumed to be negligible, so the force acting between the particles in the bulk is attractive and attributed to the van der Waals force. Therefore, particles tend to aggregate over time and the aggregates in the slurry grow as the drying time increases. However, the results of the observations of PMMA slurries confirm that the aggregates are already formed in the initial states and the structures of the aggregates do not change in the early drying stages regardless of the particle concentration. Also, in the low volatility condition, the area of the cavities reduce in the interval between 1.3–0.7 ×$d$ of the solvent height and NBA value increases slightly, although in the high volatility condition the structure organized by particles does not change in the same interval. These results imply that the effect of the drying speed upon the substrate surface coverage ratio in the last stage of the drying process support the observation results. It is expected that the differences in the degree of particle dispersion after drying that exist between the computational simulations and actual experimental results are caused by the differences in the initial aggregation states.

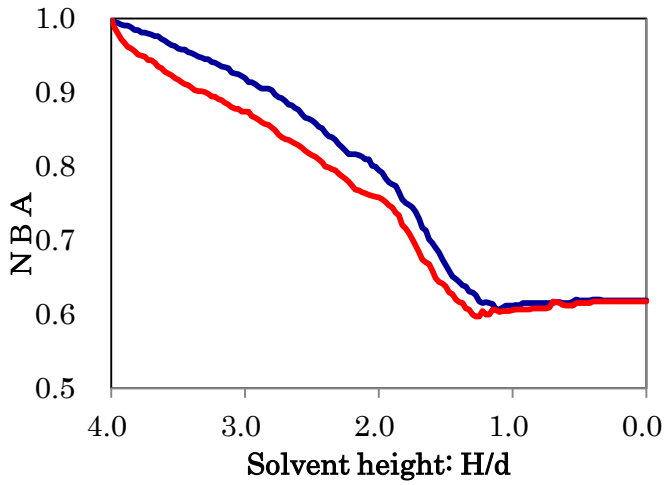


Figure 6. Evolution of the NBA values as a function of the ratio of the solvent height, H, to the particle diameter, d, using the fully dispersed state initial condition and a solvent drying speed of $5\times10^{-2}$ m/s (blue line) and $5\times10^{-3}$ m/s (red line). The initial H/d value is 4 and the final value is 0 after fully drying.

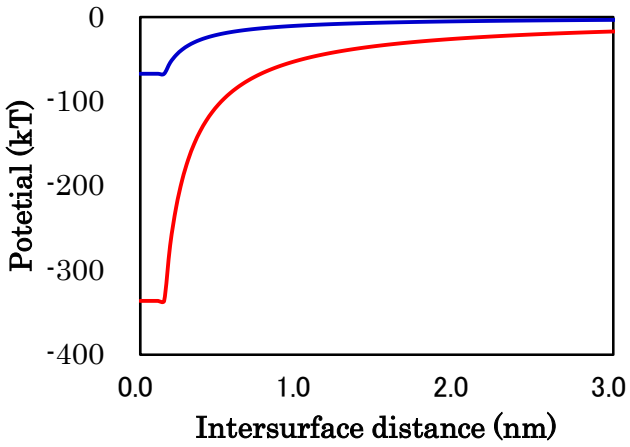


Figure 7. Calculated curve of the interparticle potential as a function of the surface separation distance for a Hamaker constant of $1\times10^{-20}$ J (blue line) and $5\times10^{-20}$ J (red line).

The change of the NBA values during the drying process under the aggregated state initial condition is shown in Fig. 8, where a clear difference does not exist between different drying speeds until a solvent height of 1.5 ×*d*. Indeed, until the solvent height reaches ~3.0 ×*d*, the NBA values under both drying speed conditions scarcely change and the aggregated structures are maintained, same as the drying process of the PMMA slurries. Subsequently, in the solvent height range between 1.1–1.5 ×*d*, the NBA values rise drastically for both drying speeds conditions, though the degree of the change of the NBA values in this last stage of the drying process increases with slower drying speeds. This increase of the NBA values is caused by the collapse of the aggregates, which corresponds well with the observation of the PMMA slurries. The results of the computational simulations under the aggregated state initial condition possess specific features that are observed in the actual drying process of PMMA slurries, so it is apparent that this condition adopted in the calculations closely reflects the real condition. When the NBA values are at a minimum in the simulations, which occurs in the final drying states, the lower portion of the aggregates are in contact with the substrates and their upper portions protrude from the interface. These results support the hypothesis regarding the mechanism of the aggregate collapse as derived from the experimental results, in which it is supposed that the aggregates are crushed vertically on the substrate by the capillary force.

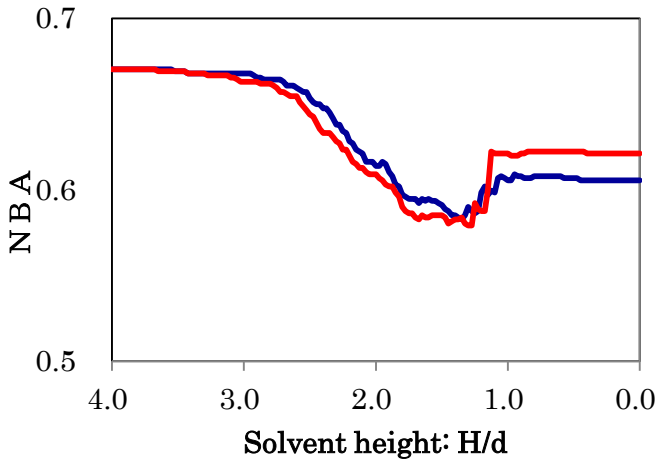


Figure 8. Evolution of the NBA values as a function of the ratio of the solvent height, H, to the particle diameter, d, using the aggregated state initial condition and a solvent drying speed of $5\times10^{-2}$ m/s (blue line) and $5\times10^{-3}$ m/s (red line). The initial H/d value is 4 and the final value is 0 after fully drying.

The simulation results obtained using the low Hamaker constant is similar to the results found during the experimental drying process of the PDMS silicone slurries. The cohesion force between particles with a low Hamaker constant is small, as is shown in the potential curve in Fig. 7, so such particles form fragile flocs. Even the weak force is able to crush the floc easily, so flocs composed of particles with a low Hamaker constant break apart owing to the vertical component of the capillary force and the particles are then packed closely by the lateral capillary force regardless of solvent conditions. It is supposed that the differences between the arrangements of the PDMS and the PMMA particles after drying are caused by the difference between the magnitudes of the existing van der Waals forces.

## 6. Conclusions

It is confirmed from the experimental and computational simulation results that the magnitude of the van der Waals force between the particles and the drying speed of the solvent are important for obtaining a coating layer with spread and highly-ordered particles on substrate after drying. The aggregated particles are pressed against the substrate by the vertical component of the capillary force, which is exerted in a contact line between the particle and the solvent at the last stage of drying. However, a weak van der Waals force creates a fragile aggregate and a slow drying speed induces a long pressing time, so with these conditions the aggregates collapse and the particles spread on the substrate. The drying simulator is found to be effective for predicting particle ordering during the drying process. So it is

supposed that this drying simulator can be a useful tool to assist in the formulations designs for liquid foundation and other cosmetic products.

## References


[1] Yagi K., Ogawa K., Kanemaru T., Joichi K., Kunizawa N., Takano R., Optical rejuvenating makeup using an innovative shape-controlled hybrid powder, IFSCC Magazine, 9 (2006)

[2] Nakamura N., Takasuka Y., Takatsuka I., Blurring of wrinkles through control of optical properties, J. Soc. Cosmet. Chem. Japan, 21 (1987) 2, 119-126.

[3] Uehara K., Minami K., Iwamoto H., Osada M., Igarashi T., Nakano K., OOsaki K., Uematsu T., Nojiri N., Kashimoto A., Fukuda K., Development of youthful-looking makeup foundation by controlling transmitted light, J. Soc. Cosmet. Chem. Jpn, 44 (2010) 48-56.

[4] Tanaka H., Enomoto N., Production procedure and cosmetic application of flaky powder, Japanese PAT. 2784261, 1998.

[5] Nishimura H., Development of new powder for “mizumizushii”-looking makeup foundation, Fragrance Journal, 34 (2006) 49-52.

[6] Ogawa K., Development of a functional pearl pigment that can provide a transparent and comfortable finish and its application, Fragrance Journal, 31 (2003) 4, 17-21.

[7] Ogawa K., Joichi K., Kanemaru T., Sakurai O., Machida A., Development of a hybrid powder that is coated with nano-fiber type-ZnO and can yield excellent optical and physical characteristics, and its application, J. Soc. Cosmet. Chem. Jpn., 39 (2005) 3, 209-213.

[8] Katsuyama T., Kimura A., Yamaguchi M., Yoshida M., Development of novel thin layered material based on a new photocomplementary color theory and its application in cosmetic foundation, Proceedings at the 19th IFSCC International Congress (1996) 123-127.

[9] Igarashi T., Recent technical trends on cosmetic foundation, Fragrance Journal, 34 (2006) 6, 17-28.

[10] Tsukiyama F., Tomita Y., Development of the functional powder responding to market trends and its application for the make-up products, Fragrane Journal, 41 (2013) 3, 47-54.

[11] Sumiyoshi A., Kumei T., Nishimoto K., Tanaka T., Liu X., Yin S., Sato T., Development of a powder with long lasting effects, J. Soc. Cosmet. Chem. Jpn., 45 (2011) 4, 315-322.

[12] Watabe K., Kumei T., Yin S., Sato T., The preparation and characterization of various-shaped cerium dioxide and its application to cosmetics, J. Soc. Cosmet. Chem. Jpn., 48 (2014) 1, 11-18.

[13] Iida M., Asami C., Nishikawa S., Development of makeup products which reproduce the radiance from inside the skin, J. Soc. Cosmet. Chem. Jpn., 47 (2013) 1, 26-32.

[14] Tsugita T., Iwai T., Makeup skin analysis using a visible RGB-LED optical coherence tomography, Fragrance Journal, 41 (2013) 3, 36-41.

[15] Katsuyma T., Hasegawa K., Proceeding of Optics and Photonics Japan 2012.

[16] Nanba M., Introduction of UV curing type ink and the future view, J. Jpn. Soc. Colour Mater., 85 (2012) 2, 72-79.

[17] Ishi M., Fabrication of polymer-immobilized colloidal crystal films by spray-coating, J. Jpn. Soc. Colour Mater., 85 (2012) 5, 196-200.

[18] Tand C., VanSlyke S. A., Appl. Phys. Lett., 51 (1987) 913-915.

[19] Burroughes J. H., Bradley D. D. C., Brown A. R., Marks R. N., Mackay K., Friend R. H., Brun P. L., Holms A. B., Nature, 347 (1990) 539-541.

[20] Dickinson E., An Introduction to Food Colloids, Oxford Univ. Press, 1992.

[21] Kumar A., Whitesides G. M., Appl. Phys. Lett., 63 (1993) 2002.

[22] Mino Y., Watanabe S., Miyahara M., Fabrication of colloidal grid network by two-step convective self-assembly, Langmuir, 27 (2011) 5290-5295.

[23] Kim H. S., Lee C. H., Sudeep P. K., Emrick T., Crosby A. J., Nanopaticle stripes, grids, and ribbons produced by flow coating, Adv. Mater., 22 (2010) 4600-4604.

[24] Fujita M., Yamaguchi Y., Development of three-dimensional structure formation simulator of colloidal nanoparticles during drying, J. Chem. Eng. Jpn., 39 (2006) 1, 83-89.

[25] Fujita M., Yamaguchi M., Simulation of 3D crystallization of colloidal nanoparticles on a substrate during drying, Intern. Polymer Processing, 22 (2007) 1, 16-21.
[26] Israelachivili J. N., Intermolecular and Surface Forces; 3rd Edition, Elsevier, Netherlands, (2011).
[27] Kralchevsky P. A., Nagayama K., Particles at Fluid Interfaces and Membranes: Attachment of Colloid Particles and Proteins to Interfaces and Formation of Two-Dimensional Arrays, Elsvier, Netherlands, (2001).
[28] Fujita M., Koike O., Yamaguchi Y., Direct simulation of drying colloidal suspension on substrate using immersed free surface model, J. Comput. Phys., 281 (2015) 421-448.

Katsuyuki Hasegawa

Basic Research Center, Shiseido CO., LTD.
2-2-1, Hayabuchi, Tsuzuki-ku, Yokohama, 224-8558, Japan
katsuyuki.hasagawa@to.shiseido.co.jp

Akio Nasu

Basic Research Center, Shiseido CO., LTD.
2-2-1, Hayabuchi, Tsuzuki-ku, Yokohama, 224-8558, Japan
akio.nasu@to.shiseido.co.jp

Masahiro Fujita

Department of Mathematics, Faculty of Science, Josai University
3-26, Kioi-cho, Chiyoda-ku, 102-0094, Japan
fujita@josai.ac.jp